Numerical investigation of local aerosol deposition in a real scale T-junction of a ventilation network

R. Ploix, E. Gehin, Jeanne Malet

Numerical investigation of local aerosol deposition in a real scale T-junction of a ventilation network

R. Ploix[1,2*], E. Gehin[1] and J. Malet[2]

[1] CERTES, Université Paris Est-Créteil, Créteil, France
[2] Institut de Radioprotection et de Sûreté Nucléaire (IRSN), PSN-RES/SCA/LEMAC, F-91400, Saclay, France

[*]E-mail : remy.ploix-upec@irsn.fr

Abstract. Local particle deposition measurements in a T-junction of a real scale ventilation network are studied and interpreted using RANS CFD simulations. To assess the validity of the simulation, an analysis of the flow at different scales is proposed. The experimental results show a particle deposition tendency to be higher downstream the T-junction and particularly on the outer side of the T-junction. This tendency appears to be linked to a separation downstream the T-junction, with the main flow on the outer side of the junction and secondary flow on the inner side. This separation seems to have an impact on the aerosol repartition in the bulk, which can be linked to aerosol concentrations gradient downstream the T-junction.

Keywords: Computational Fluid Dynamics, multi-phase Flows, turbulence, deposition, singularity, T-junction

1. Introduction

Aerosol deposition in ventilation ducts plays a key role in particulate pollution transfer in industrial facilities. It represents the natural aerosol retention (self-deposition) capacity of a ventilation network and is useful to estimate the release into the environment. Moreover, in nuclear industry, it is a critical concern for workers safety and risk management. Nuclear safety experts require tools to identify preferential deposition areas within nuclear power plant's ventilation network, and to collaborate with operators to minimize the risks of radiation exposure accidents and environmental release as a side effect of another accident in the facility. However, some correlations already exist to estimate aerosol deposition in ventilation duct, but are mainly focused on straight ducts [1] and bends[2–4]. The lack of specific simple correlations for aerosol deposition in other singularities like T-junctions is a problem to evaluate the current risk of aerosol deposition in a whole ventilation network. Some studies exist on different types of junctions [5–7] for Y-junction on the lung model (laminar flow, small duct size), [8,9] for T-junction in industrials processes (conveyor, reactor, small duct size). However, the duct size and operating configuration (mixing or separation) of the junction are important parameters that have never been studied at ventilation network scale and in a mixing configuration. To do so, CFD simulation is a good way to develop such correlations and needs to be validated. This work focuses on the assessment of numerical simulations on experimental data obtained in a specifically developed

real-scale facility where detailed flow measurements and aerosol deposition inside a horizontal T-junction are performed.

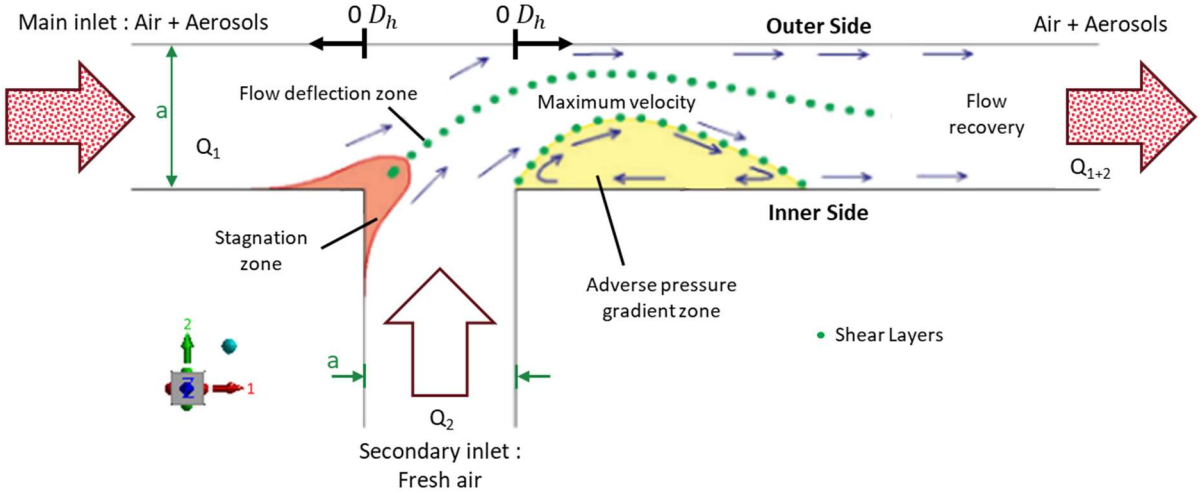

Figure 1. Scheme of the flow inside the T-junction on top view

2. Experimental procedure

Experimental results are obtained from a sixty meters long industrial size ventilation network of rectangular section (width = a = 600 mm and height = b = 400 mm) and that includes various singularities (bends, T-junctions, and converging duct). The facility and associated instrumentation are presented in [10]. The T-junction of the facility is in a mixing configuration, with two inlets and one outlet as shown on Figure 1. The main branch of the T-junction (main inlet - outlet) is located between 2 vertical bends (4 D_h upstream and downstream the secondary inlet). The experiment is conducted with aerosol injection in the main inlet (Q_1), and fresh air in the secondary inlet (Q_2). The NaCl aerosol traced with a fluorescent dye (fluorescein) is generated with a vibrating ceramic generator (named LIXEA) which provides almost monodisperse particles of 3 to 5 µm diameter number. Both inlets of the T-junction are equipped with Camfil air filter (HEPA H13). Different parameters can be studied, as flow ratios ($R = Q_1/Q_2$), shapes of T-junctions (sharp and smooth angles) and particle diameters. This paper reference case with a flow ratio $R = 3/2$, a smooth angle T-junction with 100 mm angle curvature and a particle aerodynamic diameter $d_P = 5\ \mu m$. The Reynolds number at the outlet of the T-junction is constant ($Re_{b\ out} = 235000$).

2.1. Flow measurements

The facility is equipped with PIV and hot wire anemometry for flow characterisation. For near wall velocity measurements, a Dantec Dynamics CTA measurement system (StreamLine) is used with different hot wire references (55P11, 55P15 with 5 µm diameter and 1.25 mm long plated tungsten). An OWIS motorized positioner is used to precisely move the hot wire towards the wall. For this study, it is assumed that the hot wire is at the wall position (y=0) when the CTA sends back an offline signal, indicating that the wire has broken, after touching the wall.

2.2. Aerosol measurements

The protocol developed for aerosol deposition measurement consists of manually sampling (using wipes) the deposited aerosol on 100 cm² delimited zones of the internal walls. Wipes are then analysed by fluorimetry to get the sampled mass (a calibration function exists to corelate the

fluorimeter signal with the sampled mass). More details are given in [11]. These measurements are performed at different locations upstream, downstream and inside the T-junction [12]. A total of sixteen measurements surfaces are performed, eight on the bottom wall, four on the vertical walls and four on the upper wall. For each surface, the measurement uncertainty is about 15 % for an interval of confidence of 66%.

3. Numerical procedure

The simulations are conducted on ANSYS Fluent 2022R1. Two RANS models are chosen: the k-ω SST and the RSM (ε-based). For the study, one way coupling is assumed and the lagrangian tracking method is used, with stochastic eddy interaction model [13]. This model is based on Newton's second law:

$$m_p \frac{d\overrightarrow{u_P}}{dt} = \frac{1}{\tau_p}\frac{C_D\, Re_p\, m_p}{24}(\vec{u} - \overrightarrow{u_P}) + \frac{\vec{g}\, m_p(\rho_p - \rho)}{\rho_p} + \overrightarrow{F_a} \quad (1)$$

with particle acceleration on the left side and drag force, gravity, and other forces ($\overrightarrow{F_a}$) on the right side. In equation 1, m_p is the particle mass, Re_p the particle Reynolds number, ρ_P the particle density, ρ the density of the fluid, $\vec{g}$ the gravity acceleration, τ_p the particle relaxation time and C_D the drag coefficient. The spherical drag coefficient used is C_D given by:

$$C_D = a_1 + \frac{a_2}{Re_P} + \frac{a_3}{Re_P^2} \quad (2)$$

with a_1, a_2 and a_3 constants over several range of Re_P [14].

$$Re_p = \frac{d_p|\vec{u} - \overrightarrow{u_P}|}{\nu} \quad (3)$$

$$\tau_p = \frac{\rho_p\, d_p^2}{18\ \mu} \quad (4)$$

With ν the cinematic viscosity of the fluid and μ the dynamic viscosity of the fluid. These equations assumes that the Cunningham number is equal to 1 what is valid for $d_p > 3\ \mu m$.

In the drag term of equation 1, the velocity $\vec{u}$ as a mean component $\bar{u}$ that comes from the turbulent flow calculation, and a fluctuating component U' that is modelized by the stochastic part of the particle model. The fluctuating velocity represents the interaction between a particle and a succession of eddies. These interactions are defined by the fluctuating velocity components U_1', U_2', U_3' and the duration of the interactions. These parameters are calculated as follows for the RSM case:

$$U_i' = \zeta\sqrt{\overline{u_i{}'u_i{}'}} \quad (5)$$

where ζ is a random number following a normal law, and $u_i'u_i{}'$ a Reynolds shear stress component coming from the turbulence model. For the isotropic turbulence model as k-ω SST, the following equations are considered:

$$\sqrt{\overline{u_1{}'u_1{}'}} = \sqrt{\overline{u_2{}'u_2{}'}} = \sqrt{\overline{u_3{}'u_3{}'}} = \sqrt{\frac{2k}{3}} \quad (6)$$

with k, the turbulent kinetic energy coming from the flow calculation. Thus, for the stochastic model:

$$U_1' = U_2' = U_3' = \zeta \sqrt{\frac{2k}{3}} \tag{7}$$

For the interaction time, two parameters are calculated: the eddy lifetime (t_{eddy}) and the residence time of the particle inside an eddy (t_{cross}). The lowest of these two durations is taken as interaction time.
The eddy lifetime is calculated as:

$$t_{eddy} = -\tau_L \log(r) \tag{8}$$

with r a random number between 0 and 1, and τ_L the particle lagrangian time scale. The definition of τ_L is empirical. It is defined as:

$$\tau_L = C_L \frac{k}{\epsilon} \tag{9}$$

for both turbulence models. C_L is an empirical constant with a large range of values [15,16]. The default values in Fluent are 0.15 for k-ω SST and 0.3 for RSM.
The residence time is calculated as:

$$t_{cross} = -\tau_p \, ln\left[1 - \left(\frac{L_e}{\tau_p |\vec{u} - \vec{u_P}|}\right)\right] \tag{10}$$

with L_e the eddy characteristic length, defined as :

$$L_e = \left(C_\mu\right)^{3/4} \left(k^{3/2}/\epsilon\right) \tag{11}$$

with a constant taken as $C_\mu = 0.09$, for both turbulence models.

4. Mesh sensitivity test and flow analysis

The simulation domain is the whole experimental facility. Three meshes are considered for the mesh sensitivity test, with the same wall refinement (twenty cells in the refinement zone and $y^+ \approx 1$ for the last wall cell) but different bulk element sizes (48 mm, 36 mm and 24 mm, corresponding to $0.1D_h$, $0.075D_h$ and $0.05D_h$ (D_h : hydraulic diameter) and 2.3 - 4 - 9.4 million elements). The mesh is constructed with connected topological blocks with different element types: hexahedral for straight parts, and tetrahedral for T-junction and bends.

4.1. Mesh sensitivity

The mean flow field, turbulent kinetic energy, and Reynolds stresses components at different distances downstream the T-junction are compared between the three meshes for both turbulence models. Some differences are observed in the k-ω SST calculations, but these are considered negligeable for the study. For the RSM calculations, the three meshes give the same results for the three mean velocity components and the turbulent kinetic energy. The intermediate mesh is then chosen for both turbulence models, to get a convenient computational time.

4.2. Results on straight rectangular duct

Comparisons of non-dimensional near wall streamwise turbulence $U_i' U_i'^+$ and velocity U_i^+ component are done between our numerical and experimental results at the same flow rate, on a vertical wall, in a straight duct of the facility, $7D_h$ downstream a horizontal bend. Turbulent data are presented on Figure 2A along with DNS data [17] as a reference. Flat channel data are preferred

to duct channel data since the shear Reynolds $Re_\tau = u_\tau D_h/2\nu$ (with u_τ the friction velocity) available in the literature is more adequate for flat channel. Our numerical data is $Re_{\tau\,RSM}$ = 3800 and in flat channel DNS we found $Re_{\tau\,DNS} = 4200$ in [17]. To our knowledge, the maximum shear Reynolds number in square duct that has been simulated with DNS is $Re_\tau = 1200$ in [18]. Moreover, [19] compared turbulent statistics between the bottom wall bisector from a DNS of a square duct with a DNS on a flat channel and found a good agreement despite the influence of the sidewalls.

On the Reynolds stress graph (Figure 2A), both experimental and RSM agreed for some points with the DNS, with a first peak in the buffer layer at y^+ = 15. The experimental peak in the buffer layer is lower than the numerical one. This is likely due to hot-wire filtering effects due to the probe size (the non-dimensional size of the wire l^+ is just below 30) as studied in [20,21]. The plateau (y^+ = 100) that is visible on experimental and DNS data increases with Re_τ [22,23]. This plateau is not visible on RSM modelling which can be a limitation of the numerical model.

Considering the experimental uncertainties (wall position [24], probe alignment with the wall [25]) and the proximity of a singularity ($7D_h$ downstream of a horizontal bend), the experimental and numerical near-wall non-dimensional streamwise velocity profiles are in good agreement together and with the classical boundary layer profile [26]. Such results in the boundary layer in a real industrial facility with a commerical software give a lot of confidence in the chosen approach, which uses CFD to produce correlations for T-junctions. It is also demonstrated that almost canonical flows can be recovered in this industrial facility.

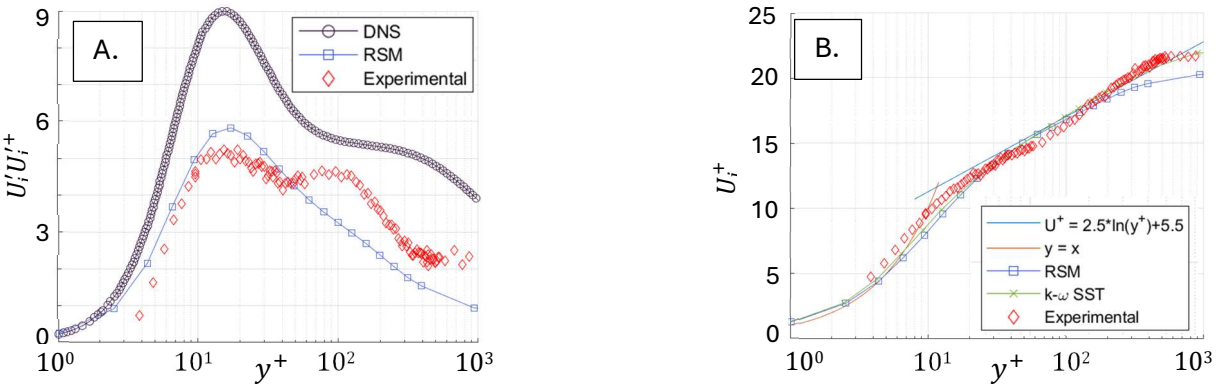

Figure 2. Experimental and numerical horizontal near wall profiles of $U_i'U_i'^+$ (left) and U_i^+ (right), 7 D_h downstream a horizontal bend

4.3. Results on rectangular T-junction

In the T-junction, the secondary injection creates an adverse pressure gradient zone. This zone is visible on Figure 4 : on the streamwise component U_1 a low velocity region appears on the side of the secondary injection downstream the T-junction ; on the turbulent kinetic energy (k) part, a peak is visible behind the T-junction, directly followed by a low turbulent kinetic energy zone. This zone is also visible on the near wall streamwise velocity profiles downstream the T-junction presented on Figure 3 for both turbulence model. It is noted that k-ω SST model assesses that $3D_h$ downstream the T-junction, the impact of the singularity on the near wall velocity profile is negligible, since for RSM model, the impact is still visible. These modifications of the shape of near wall velocity profiles will lead to a different presentation for aerosol deposition that can be seen in the literature. Generally, aerosol deposition is determined based on a non-dimensional deposition velocity calculated from the friction velocity ($u^* = \sqrt{\tau_\omega/\rho}$ with τ_ω the wall shear stress and ρ the fluid density). Most of the aerosol studies on deposition estimate this friction velocity by pressure drop measurements [27], which is thus determined as a global parameter for the whole

duct section between the two pressure measurements points. However, as soon as local deposition is considered inside a complex geometry, a local friction velocity should be used for the non-dimensional deposition velocity. The local friction velocity can experimentally be obtained through standard near wall velocity profiles with the Clauser chart method [28]. Nevertheless, near wall velocity profile in the T junction is far from standard profile (Figure 3) what makes this method unusable. Thus, the chosen deposition parameter used here is defined as the ratio of the deposited mass on a surface (m_k) by a reference mass (m_{ref}) defined here as the deposited mass on a reference surface of the same wall as:

$$M_k = \frac{m_k}{m_{ref}} \tag{12}$$

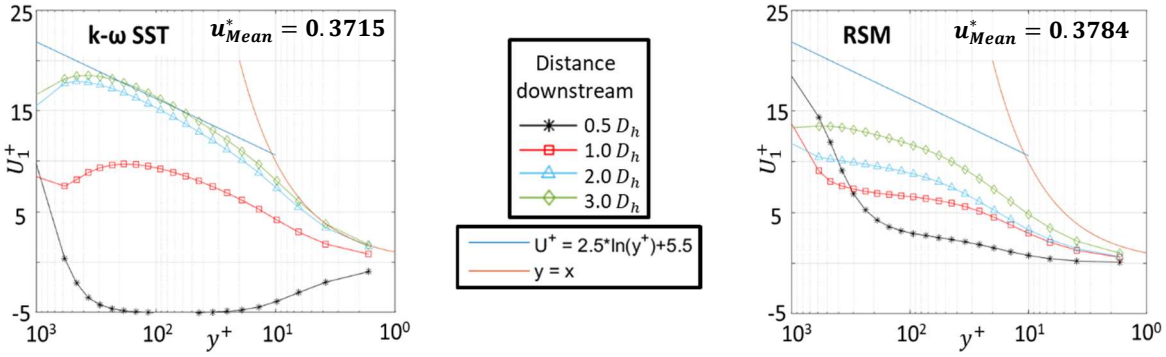

Figure 3. Near wall horizontal streamwise velocity profiles at different distances downstream the T-junction calculated using a mean friction velocity on the straight duct downstream the T-junction, compared to standard velocity profiles

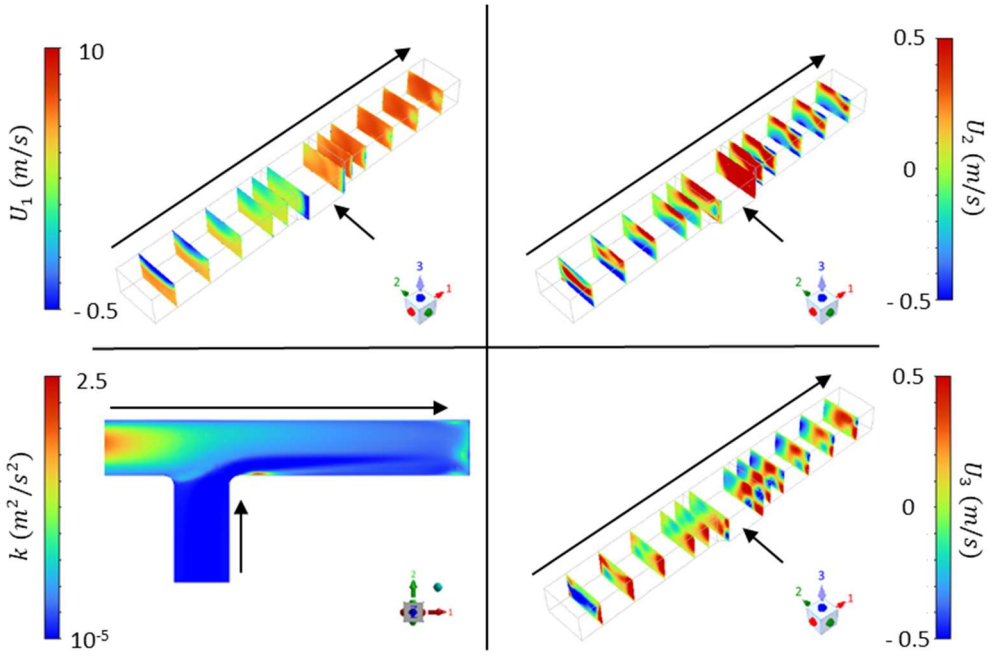

Figure 4. RSM simulation view of the three velocity components and turbulent kinetic energy at mid height in the T-junction

A first result is that there is much more aerosol deposition on the bottom wall (floor) of the duct than on the other walls (vertical and top one) [2]. Thus, most of the measurement surfaces are on the floor of the duct. Figure 5 shows the experimental deposition results on the bottom

wall of the reference case (the reference surface of eq. (12) is circled in red). The deposition downstream the T-junction is increased compared to the deposition inside the singularity. Downstream the T-junction, an enhanced deposition is visible on the outer side compared to the inner side. To our knowledge, these two effects have never been measured in previous studies. They are linked to the flow downstream the T-junction, which can be studied using our numerical results presented on Figure 4. On the transverse velocity component U_1 and U_2 part (Figure 4), there is a vortex in the whole duct upstream the T-junction which is induced by a vertical bend upstream [29]. Downstream the T-junction, this vortex seems compressed on the outer side of the flow with smaller structures on the inner of the flow in the incoming secondary flow. The mixing zone between the primary and the secondary flow is visible on the turbulent kinetic energy field. Due to the secondary flow inlet, a region of low turbulent kinetic energy on the inner side of the flow appears, where the experimental deposition is the lowest downstream the T-junction on Figure 5. The compression of the flow from the main inlet on the outer side of the duct downstream the singularity also impacts the aerosol repartition in the duct downstream the T-junction. Figure 6 shows a top view of steady-state particle trajectories inside the T-junction based on an RSM flow calculation. A significant difference on aerosol trajectories repartition is visible downstream the T-junction. This difference can be linked to an aerosol concentration gradient that can explain the experimental results presented on Figure 5.

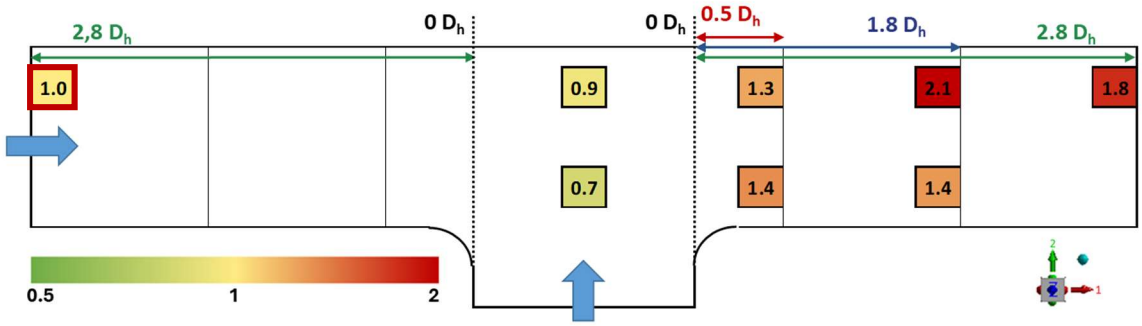

Figure 5. Experimental aerosol deposition on the bottom wall (floor) of the T-junction of the facility (top view), with the reference surface of eq. (12) circled in red

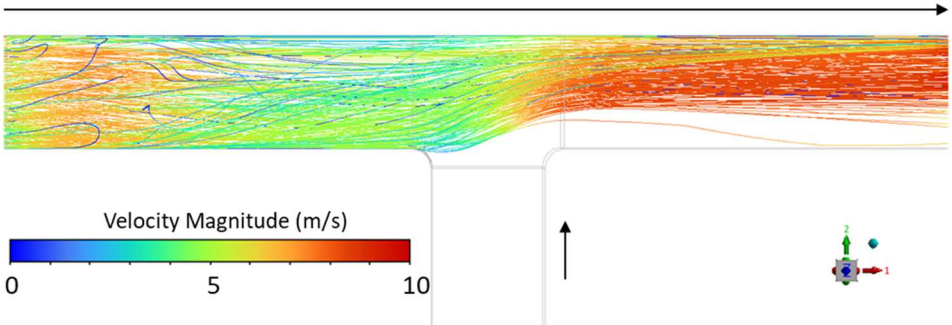

Figure 6. Top view of steady state particle trajectories inside the T-junction based on an RSM flow calculation

5. Conclusion

Aerosol deposition measurements in a real scale ventilation T-junction are conducted for the first time and studied using RANS-RSM and k-ω SST associated simulations. Near wall velocity and Reynolds stresses profiles from these simulations are compared with both our experimental data and DNS data from the literature. Such dedicated characterisation of the flow is not usual in aerosol deposition studies [3,27]. An increased deposition downstream the T-junction on the

bottom outer side of the flow is linked to separated flow downstream the T-junction, which shall increase the aerosol concentration in the outer side due to the flow coming from the secondary inlet. The increased aerosol bulk concentration on the outer side is obtained in the numerical simulation and could be experimentally verified with bulk aerosol concentration measurement downstream the T-junction. This work shows that detailed measurements allow to assess the validity of CFD simulation that can then be used to develop simplified correlations for industrial cases.

6. References

[1] M. R. Sippola, W. W. Nazaroff, *Aerosol Science and Technology* **2005**, *39*, 139–150.
[2] D. Costa, UPEC, Créteil, **2022**.
[3] M. Ben Othmane, M. Havet, E. Gehin, C. Solliec, *Aerosol Science and Technology* **2010**, *44*, 775–784.
[4] H. Lu, Y. Wang, *Build. Simul.* **2019**, *12*, 723–734.
[5] C. S. Kim, D. M. Fisher, D. J. Lutz, T. R. Gerrity, *J. Aerosol Sci.* **1994**, *25*, 567–581.
[6] R. Gupta, A. R. McFarland, *Aerosol Science and Technology* **2001**, *34*, 216–226.
[7] I. Balashazy, W. Hofmann **1995**.
[8] Y. Doroshenko, J. Doroshenko, V. Zapukhliak, L. Poberezhny, P. Maruschak, *Transport* **2019**, *34*, 19–29.
[9] R. Khan, M. Wieczorowski, A. H. Seikh, I. A. Alnaser, *Engineering Science and Technology, an International Journal* **2024**, *52*, 101683.
[10] J. Malet, M. Radosavljevic, M. Mbaye, D. Costa, J. Wiese, E. Gehin, *Building and Environment* **2022**, *222*.
[11] D. Costa, J. Malet, E. Géhin, *Meas. Sci. Technol.* **2022**, *33*, 94001.
[12] R. Ploix, J. Malet, E. Gehin (Eds.) *Etude des phénomènes locaux sur le dépôt des aérosols dans les conduits de ventilation*, CFA 2023, **2023**.
[13] D. I. Graham, P. W. James **1996**, *22*, 157–175.
[14] S. A. Morsi, A. J. Alexander, *J. Fluid Mech.* **1972**, *55*, 193.
[15] E. A. Matida, W. H. Finlay, C. F. Lange, B. Grgic, *Aerosol Science* **2004**, *35*, 1–19.
[16] L. Tian, G. Ahmadi, *Journal of Aerosol Science* **2007**, *38*, 377–397.
[17] M. Lee, R. D. Moser, *J. Fluid Mech.* **2015**, *774*, 395–415.
[18] H. Zhang, F. X. Trias, A. Gorobets, Y. Tan, A. Oliva, *International Journal of Heat and Fluid Flow* **2015**, *54*, 258–267.
[19] S. Gavrilakis, *J. Fluid Mech.* **1992**, *244*, 101.
[20] C. Chin, N. Hutchins, A. Ooi, I. Marusic, *Exp Fluids* **2011**, *50*, 1443–1453.
[21] F. Ghanadi, L. Djenidi, *Exp Fluids* **2021**, *62*.
[22] B. C. Khoo, Y. T. Chew, C. J. Teo **2000**, *29*, 448–460.
[23] J. F. Morrison, B. J. McKeon, W. Jiang, A. J. Smits **2004**, *508*, 99–131.
[24] R. Örlü, J. H. Fransson, P. H. Alfredsson **2010**.
[25] A. Segalini, A. Cimarelli, J.-D. Rüedi, E. de Angelis, A. Talamelli, *Meas. Sci. Technol.* **2011**, *22*, 105408.
[26] H. Schlichting, K. Gersten, *Boundary-Layer Theory*, Springer Berlin Heidelberg; Imprint: Springer, Berlin, Heidelberg, **2017**.
[27] M. R. Sippola, W. W. Nazaroff, *Aerosol Science and Technology* **2004**, *38*, 914–925.
[28] F. H. Clauser in *Advances in Applied Mechanics*, Elsevier, **1956**, pp. 1–51.
[29] P. Rudolf, M. Desová, *Applied and Computational Mechanics* **2007**, *1*, 255–264.